Three-dimensional Child–Langmuir law for uniform hot electron emission

W. S. Koh and L. K. Ang[a)]
School of Electrical and Electronic Engineering, Nanyang Technological University, Singapore 639798, Singapore

T. J. T. Kwan
Applied Physics Division, Los Alamos National Laboratory, Los Alamos, New Mexico 87545

(Received 10 November 2004; accepted 22 March 2005; published online 13 May 2005)

This paper presents a three-dimensional (3D) model of Child–Langmuir (CL) law for uniform hot electron emission in planar and cylindrical gap, including the effects of finite emission energy. It is found that the enhancement of 3D CL law (in terms of 1D CL law) can be written in a general form of $J_C[3D]/J_C[1D]=1+F\times G$, where F is the normalized mean position of 1D electron flow in classical, weakly relativistic, and quantum regime, and G is the geometrical correction factor depending on the geometrical properties of the finite emitting patches on the cathode. In particular, we present the analytical solutions for various emitting patches, such as rectangle, ellipse, square, circle, triangle, and polygon, which agree very well with 3D particle-in-cell simulation. For a cylindrical gap of finite width, it is also found that the convergent flow (cathode outside) has larger enhancement than the divergent flow (cathode inside) at a given aspect ratio of outer radius to inner radius of the gap. Smooth transition from various operating regimes is demonstrated. © *2005 American Institute of Physics*. [DOI: 10.1063/1.1913612]

I. INTRODUCTION

The interaction of intense charged particle in a gap has remained an area of considerable interests in high current diodes, high power microwave sources, accelerator physics, vacuum microelectronics, and sheath physics. One of the important aspects of intense beam-gap interactions is the space-charge limited current density, which is also known as Child–Langmuir (CL) law.[1] The CL law gives the maximum current density allowed for steady-state electron beam transport across a gap with gap spacing D and gap voltage V_g, before a virtual cathode is formed near the emitting surface. The classical CL law is essentially a one-dimensional (1D) law for nonrelativistic electron flow across a planar gap at zero emission velocity, and it is given by

$$J_C(1D)=\frac{4\epsilon_o}{9}\sqrt{\frac{2e}{m}}\frac{V_g^{3/2}}{D^2}, \tag{1}$$

where e and m are the charge and mass of the electron, respectively, and ϵ_o is the permittivity of free space.

The 1D classical CL law [Eq. (1)] had also been extended to include the effects of finite emission velocity (hot electron emission),[2] to a relativistic model (without self-magnetic field),[3] and a coaxial cylindrical configuration.[4] It is also found that quantum effects,[5–7] such as electron tunneling and electron exchange correlation becomes important when the size of the gap decreases to nanometer scale, and the gap voltage is comparable to the Hartree energy level. A new quantum scaling of $V_g^{1/2}$ and D^{-4} has also been calculated numerically[5] and derived analytically.[6]

In addition to the 1D models, the extension of the classical 1D planar CL law to two-dimensional (2D) models has been a subject of much interest in recent years.[8–13] For uniform cold electron emission, a 2D planar classical CL law has been derived analytically,[8] which agrees well with the simulation results.[9] Enhanced emission near to the beam edges has also been reported in various 2D nonuniform emission models.[10–13] These 2D classical CL models are focused only on simple 2D finite emitting patches with cold electron emission, where the effects of finite emission energy, 3D emitting patches, and curvature of the electrodes are not included. The 2D classical CL law for a cylindrical gap with finite width has also been simulated[14] and derived,[15] but both findings are limited and contain some discrepancies. Simple extension of the classical 2D CL models to other regimes, such as relativistic and quantum regime has not been developed.

Thus, in this context, several questions arise: How does one derive a 3D uniform CL law that is valid in classical, relativistic, and quantum regime for planar and cylindrical models? What are the analytical scalings for various 3D emitting patches, such as triangle, rectangle, ellipse, square, circle, and polygon? Is the effect of finite emission energy important in multidimensional CL law? This paper addresses these questions.

II. THEORY AND SIMULATION

Consider electrons with monoenergetic emission energy E_0 injected uniformly and normally into a planar gap with gap spacing D, where the cathode ($z=0$) is grounded and the anode ($z=D$) is held at a dc voltage V_g. The emission of electrons from the cathode is confined to a finite and well-defined emitting patch (i.e., rectangle or ellipse), which is characterized by two parameters: a and $b\leqslant a$. For example, an ellipse has semiaxes of a and b, and a rectangle has a length $L=2a$ and width of $W=2b$.

[a)]Electronic mail: elkang@ntu.edu.sg

Using Lau's methodology,[8] we may calculate the enhancement of the 3D limiting current density $J_C(3D)$ with respect to the 1D limiting current density $J_C(1D)$, which is defined as $\mu = J_C(3D)/J_C(1D)$. In the limit of large emitting area as compared to the gap spacing ($a \geqslant b \gg D$), we obtain a general expression of μ:

$$\mu = 1 + F \times G. \tag{2}$$

Here, G is the geometrical correction parameter, which depends on a/D and b/D for various types of emitting patches. The mean-position correction factor $F \equiv \int_0^1 \overline{z} n(\overline{z}) d\overline{z} / \int_0^1 n(\overline{z}) d\overline{z}$ is the mean position (in terms of D) of the 1D electron flow, and it depends on the electron flows in classical, weakly relativistic, and quantum regime, where $\overline{z} = z/D$ and $n(\overline{z})$ is the 1D electron density distribution function that can be calculated by solving 1D Poisson equation and equation of motion at its corresponding $J = J_C(1D)$ condition. Note that F is independent of the geometrical parameters such as a/D and b/D, as $n \approx n(\overline{z})$ has been used in the derivation by expanding $a \geqslant b \gg D$ to the first order of magnitude (see below).

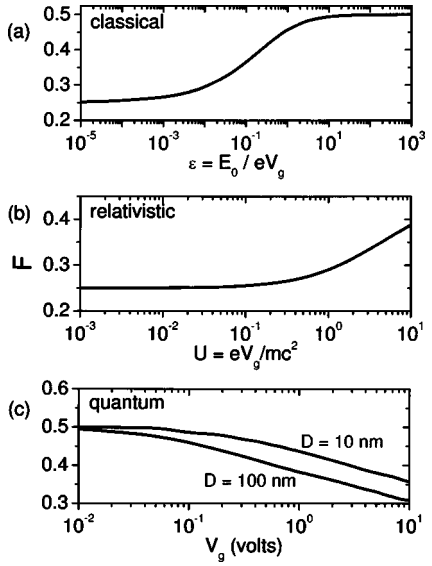

FIG. 1. The mean-position correction parameter: F (solid lines) as a function of (a) $\epsilon = E_0/eV_g$ in classical regime, (b) $U = eV_g/mc^2$ in relativistic regime at $\epsilon = 0$, (c) V_g (V) for $D = 10$ nm (top) and 100 nm (bottom) in quantum regime at $\epsilon = 0$.

A. Mean-position factor *F*

Classical. For a finite normalized emission energy $\epsilon = E_0/eV_g$, the classical 1D CL law is enhanced by a factor of $(\sqrt{\epsilon+1}+\sqrt{\epsilon})^3$.[2] To calculate F at finite ϵ, we numerically solve the 1D normalized Poisson equation (coupled with the equation of motion) in the classical regime,

$$\phi'' = \frac{4}{9}\frac{(\sqrt{\epsilon+1}+\sqrt{\epsilon})^3}{\sqrt{\epsilon+\phi}} \tag{3}$$

with the boundary conditions: $\phi(0) = 0$, $\phi(1) = 1$, and $\phi'(0) = \alpha \leqslant 0$. Here, the prime denotes the derivative with respective to $\overline{z}$, $\phi = V/V_g$ is the normalized electric potential and α (a function of ϵ) is the surface electric field at the cathode emitting at space charge limited condition. The mean-position correction factor F is calculated by using $n(\overline{z}) \sim 1/\sqrt{\phi(\overline{z})+\epsilon}$, where $\phi(\overline{z})$ is obtained from solving Eq. (3) for a given $\epsilon \geqslant 0$. In the limit of zero emission energy ($\epsilon = 0$), we have $\alpha = 0$, $n(\overline{z}) \sim \overline{z}^{-2/3}$, and thus $F = 1/4$. Figure 1(a) shows the calculated F as a function of ϵ in classical regime. At small emission energies ($\epsilon \ll 1$), the solution approaches the limit of $F = 1/4$, as indicated by the classical CL law. For large ϵ, the electrons propagate across the gap without significant acceleration and the electron density remains a constant in the gap. Therefore, $F \to 1/2$ when $\epsilon \gg 1$.

Relativistic. By including the relativistic effect at zero emission energy (but ignoring the self-magnetic field),[3] F is calculated by solving the Poisson equation and relativistic equation of motion. The solution for F is

$$F(u) = \frac{1}{4}\frac{\int_0^1 Q(w,u)dw}{Q(1,u)}, \tag{4}$$

where $Q(w,u) = \int_0^1 (p^2/\sqrt{1+uwp^4})dp$, w and p are dummy variables, $u = (1+eV_g/mc^2)^2 - 1$, and c is speed of light. In Fig. 1(b), F is plotted as a function of $U = eV_g/mc^2$ up to $U = 10$. It is clearly shown that the solution recovers to the classical limit of $F = 1/4$ at $U \to 0$. In the weakly relativistic regime ($U < 1$), assuming the self-magnetic field is negligible, Eq. (4) is approximately

$$F = \frac{1}{4}\left(1 + \frac{3U}{28}\right), \tag{5}$$

which agrees well with numerical results up to $U \approx 0.8$. Note in the highly relativistic regime ($U \gg 1$), the electron travels close to speed of light with a constant density, and thus $F = 1/2$ (not shown) if the self-magnetic field can be ignored.

Quantum. When the gap spacing is on the order of the electron de Broglie wavelength, and the gap voltage is smaller or comparable to the Hartree energy, quantum effects such as electron tunneling and electron exchange correlation becomes important.[5] Using mean-field theory and local density approximation, we solve the time-independent Schrödinger and Poisson equations to obtain n, and thus F for various small V_g and D. Figure 1(c) shows the calculated F as a function of V_g(=0.01–10 V) for $D = 10$ nm (top) and $D = 100$ nm (bottom). At deeply quantum regime where the electron tunneling and exchange correlation are dominant, we have $F = 1/2$ at $V_g < 0.1$ V for small $D < 100$ nm. When the electron de Broglie wavelength is much smaller than the gap spacing, it recovers the classical limit of $F = 1/4$.[5]

B. Geometrical factor *G*

To calculate the geometrical correction factor G, we consider two types of emitting patches on a planar cathode: (i) rectangle and (ii) ellipse. Consider a planar cathode with a rectangular or elliptical emitting patch of length $L = 2a$ and width $W = 2b$, separated from the anode by gap spacing D. In the model, the cathode is located at $z = 0$, and the anode is situated at $z = D$. Electrons are emitted from the finite emitting area, $-a < x < a$ and $-b < y < b$, with a uniform current density J. For a large emitting patch ($a \geqslant b \gg D$), the virtual cathode will occur first at the center of the emitting patch

when J reaches the space-charge limited condition. The calculation of the space-charge field is thus focused along the centerline in the middle of the emitting area, which is perpendicular to the cathode and anode. As J is increased to the space-charge limited current density J_C the electric field near to the cathode along the centerline is driven to (or less than) zero, and thus virtual oscillations set in and emitted electrons are reflected back to the cathode.

In derivation of G, we have used the methodology similar to the 2D CL law derived by Lau.[8] Here, we will only show the derivation of a rectangular emitting patch in a planar gap. Consider an incremental charge emerging from the center of the rectangular emission area is $en(x,y,z)\Delta x\Delta y\Delta z$, where $n(x,y,z)$ is the electron density. The change in electric field along the incremental charge is then given by

$$\Delta E = \frac{en(x,y,z)\Delta x\Delta y\Delta z}{4\pi\epsilon_0(x^2+y^2+z^2)}. \tag{6}$$

Considering only the normal component of the electric field, we multiply Eq. (6) by the directional cosine, $z/(x^2+y^2+z^2)^{1/2}$. By integrating Eq. (6) over the entire volume of uniform electron flow, the surface electric field at the center of the emitting patch due to the space charge within the gap is

$$E = \frac{e}{\pi\epsilon_0}\int_0^1 \bar{z}d\bar{z}\int_0^{\bar{b}} d\bar{y}\int_0^{\bar{a}} \frac{n(\bar{x},y,z)d\bar{x}}{(\bar{x}^2+\bar{y}^2+\bar{z}^2)^{3/2}}, \tag{7}$$

where $\bar{x}=x/D$, $\bar{y}=y/D$, $\bar{z}=z/D$, $\bar{a}=a/D$, and $\bar{b}=b/D$ are normalized parameters. Under the limit of $a\gg b\gg D$, we assume $n(\bar{x},\bar{y},\bar{z})\approx n(\bar{z})$, and Eq. (7) becomes

$$E \approx \frac{e}{2\epsilon_0}\int_0^1 d\bar{z}n(\bar{z})\left(1-\frac{2}{\pi\bar{b}}\sqrt{1+k^2\bar{z}}\right), \tag{8}$$

where $0\leqslant k=b/a=W/L\leqslant 1$.

For a fixed current density $J\sim n(\bar{z})\sqrt{\phi(\bar{z})+\epsilon}$, we equate the surface electric field at $J=J_C[3D]$ and $J=J_C[1D]$ to obtain the enhancement factor

$$\mu = \frac{J_C[3D]}{J_C[1D]} = 1+\frac{2}{\pi\bar{b}}\sqrt{1+k^2}\times F, \tag{9}$$

where $F\equiv\int_0^1\bar{z}n(\bar{z})d\bar{z}/\int_0^1 n(\bar{z})d\bar{z}$ is the mean normalized position of the electron flow from the cathode, which is shown in Fig. 1. In comparison to Eq. (2), the geometrical correction factor G is

$$G = \frac{2}{\pi}\frac{\sqrt{1+k^2}}{b/D} = \frac{4}{\pi}\frac{\sqrt{1+k^2}}{W/D} \text{ (rectangle)}. \tag{10}$$

Similarly, for an elliptical emission area, with long radius a, and short radius b on the planar cathode, the analytical G is

$$G = \frac{2}{\pi}\frac{E(\xi)}{b/D} \text{ (ellipse)}, \tag{11}$$

where $E(\xi)$ is the complete elliptic integral of the second kind, and $0\leqslant\xi=\sqrt{1-k^2}\leqslant 1$.

At the limit of $k=1$ ($a=b$), Eqs. (10) and (11) become, respectively,

$$G = \frac{4}{\pi}\frac{\sqrt{2}}{L/D} \text{ (square)}, \quad G = \frac{1}{r/D} \text{ (circle)} \tag{12}$$

for square and circle, where $L=2b$ is the length of the square, and $r=b$ is the radius of the circle. At $k\to 0$ ($a\gg b$), Eqs. (10) and (11) are identical, which converge to become

$$G = \frac{4}{\pi W/D} \text{ (long strip)} \tag{13}$$

for an infinitely long strip of width W.[8]

Consider a square and a circle with same emission area of $A=L^2=\pi r^2$, we have $G\approx 1.8/(\sqrt{A}/D)$ for the square, and $G\approx\sqrt{\pi}/(\sqrt{A}/D)$ for the circle, which are nearly identical numerically for a fixed A. Thus, we may formulate approximately an expression of $G(m)$ for an equilateral m-sided polygon by using the expression of $G(m)=\sqrt{\pi}/(\sqrt{A(m)}/D)$, where $m=4$ and $m\gg 1$ represent a square and a circle, respectively. Let $m\geqslant 3$ be the number of vertices of a polygon with a radius of r_m and an area of $A(m)=mr_m^2/2\times\sin(2\pi/m)$. Using the approximation, we have

$$G(m) = \frac{\sqrt{2(1-\cos[2\pi/m])}}{L/D}\sqrt{\frac{2\pi/m}{\sin[2\pi/m]}}, \tag{14}$$

where L is the length of the polygon. As an example, we have $G(3)=2\sqrt{2\pi/3}/(L/D)$ at $m=3$ for an equilateral triangular emission site of length L.

C. Particle-in-cell (PIC) simulation

It is important to note that the G derived above for elliptical and rectangular emitting patches are more accurate than the postulations that have been proposed by Lau[8] and Rokhlenko.[11] For comparison, the enhancement factor is rewritten in the form of $\mu=1+C/(b/D)$ and $C=F\times G\times(b/D)$ is a constant depending on the value of $k=b/a$ as shown in Fig. 2(a) (solid lines), where $F=0.25$ (zero emission energy in classical regime) is assumed. The dash lines are the postulations (bottom and top): (i) $C=0.5/\pi+(0.25-0.5/\pi)k$ for an ellipse[8] and (ii) $C=0.16(1+k)$ for an rectangle under uniform (or average) emission model.[11] From the figure, we see that both postulations have significantly overestimated the enhancement factor C for finite values of k. Note $C=0.25$, $C=0.2251$, and $C=0.1591$ are, respectively, for circle, square, and infinitely long emitting strip.

The accuracy of the analytical G (or C) is also verified by running a 3D particle-in-cell (PIC) simulation code MAGIC3D (Ref. 16) in the classical regime at zero emission energy ($F=1/4$). Consider a planar gap with $D=1$ cm and $V_g=1$ kV, where a finite emitting patch (i.e., ellipse, rectangle, circle, square, and triangle) is created on a planar cathode to emit electrons uniformly over the entire emitting patch. A small initial energy of 0.1 eV is assumed to initiate the electron emission.

Using the overinjection method, we slowly increase the amount of emission current until a limiting current density is

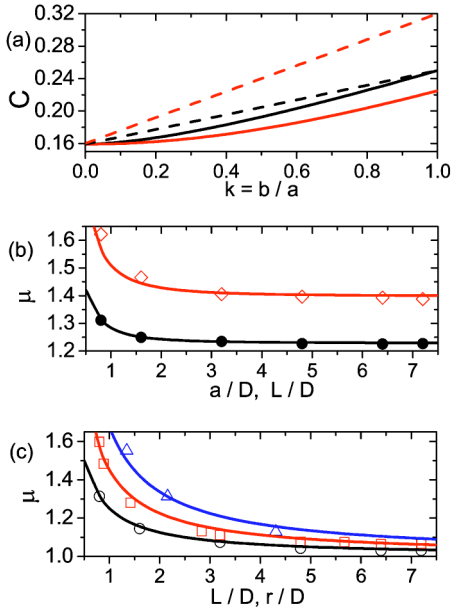

FIG. 2. (Color online). (a) The enhancement factor $C=F\times G\times(b/D)$ as a function of $k=b/a$ for ellipse (top) and rectangle (bottom). The dash lines are from Lau (Ref. 8) for an ellipse (bottom) and Rokhlenko (Ref. 11) for a rectangle (top). The enhancement of 3D Child–Langmuir (CL) law μ (in terms of 1D CL law) for (b) ellipse (a/D) and rectangle (L/D), and (c) square and triangle (L/D), and circle (r/D), where the width of rectangle and minor semiaxis of ellipse are fixed at $W/D=0.8$ and $b/D=0.8$, respectively. The symbols are 3D PIC simulation: ◇, rectangle; ●, ellipse; △, triangle; □, square; ○, circle).

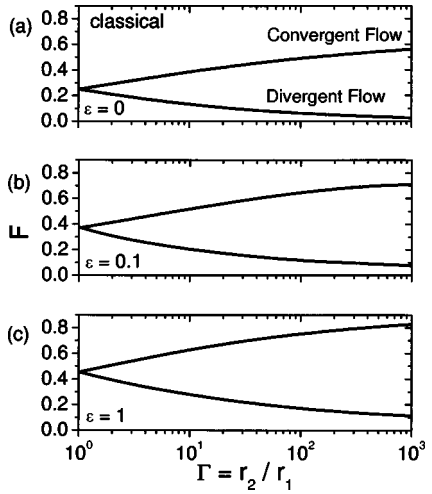

FIG. 3. The mean-position correction parameter F of a coaxial cylindrical gap of outer radius r_2 and inner radius r_1 as a function of the aspect ratio $\Gamma=r_2/r_1$ for convergent flow (top) and divergent flow (bottom) at $\epsilon=$(a), 0, (b) 0.1, and (c) 1.

reached, which is determined when the virtual cathode oscillation starts to occur near the center of the emitting patch. When the injected current density is larger than the CL limiting current density, the surface electric field normal to the cathode's center position will become time dependent, and fluctuates at around zero electric field. For a rectangular and elliptical emitting patch, the width of the rectangle, and the short radius of the ellipse are fixed at $W=0.8$ cm and $b=0.8$ cm. The length L of the rectangle, square, and triangle, the major radius a of the ellipse, and the radius r of the circle are varied from 0.8 cm to 7.2 cm. Figures 2(b) and 2(c) show the comparison of the enhancement of CL law μ between the PIC simulation (symbols) and the analytical results (solid lines) in the range of $0.8\leqslant(a/D,L/D,r/D)\leqslant 7.2$. The comparison shows excellent agreements, where the error is within 4%, and thus confirms the analytical formulas of G derived. Note in Fig. 2(b), μ recovers the 2D classical CL law when $a/D\gg 1$ and $L/D\gg 1$.

D. Cylindrical model

The formulation is extended to a 2D coaxial cylindrical model of finite width W, with outer radius r_2 and inner radius r_1. In the 1D limit of the classical cylindrical model, the space-charge limited current line density $I_{LB}(1D)$ is the 1D Langmuir–Blodgett (LB) law.[4] For simplicity, we will only focus on the classical regime, and extend the classical 1D LB law to a 2D LB law (with finite length W) for both divergent (cathode is inside) and convergent flow (cathode is outside). In the form of $1+F\times G$, the 2D classical LB law with finite normalized emission energy ϵ (in terms of 1D LB law) is

$$\frac{I_{\mathrm{LB}}(2\mathrm{D})}{I_{\mathrm{LB}}(1\mathrm{D})}=1+\frac{4/\pi}{W/D}\times F(\Gamma,\epsilon), \tag{15}$$

where $F(\Gamma,\epsilon)=\int_{R_1}^{R_1+1}g(\bar{r})n(\bar{r},\Gamma,\epsilon)d\bar{r}/\int_{R_1}^{R_1+1}n(\bar{r},\Gamma,\epsilon)d\bar{r}$ is the mean-position correction factor, and $g(\bar{r})$ measures the distance from the cathode, which are $g(\bar{r})=\bar{r}-R_1$ and $g(\bar{r})=1+R_1-\bar{r}$ for divergent flows and convergent flows, respectively. Here, $R_1=r_1/D$ is the normalized inner radius, $\Gamma=r_2/r_1>1$ is the aspect ratio between the outer radius and inner radius, $\bar{r}=r/D$, and $D=r_2-r_1$ is the gap spacing. Thus, the geometrical factor of a 2D LB law is $G=4/\pi/(W/D)$.

For a given Γ and ϵ, we solve the 1D cylindrical Poisson equation and equation of motion to obtain $n(\bar{r},\Gamma,\epsilon)\sim 1/[\bar{r}\sqrt{\phi(\bar{r},\Gamma,\epsilon)+\epsilon}]$, which gives $F(\Gamma,\epsilon)$ for both convergent (top) and divergent flows (bottom) as shown in Fig. 3 at various $\epsilon=0$, 0.1, and 1. At $\Gamma\to 1$, both convergent and divergent flows recover the 2D planar limit where F depends only on ϵ as shown in Fig. 1(a). In this limit, Eq. (15) recovers the scaling of an infinitely long planar emitting patch of width of W [cf. Eq. (13)], and thus gives a *smooth* transition between the 2D CL law and 2D LB law (see below).

It is interesting to see that the dependence of Γ is different for divergent and convergent flows, where the former (latter) decreases (increases) with increasing Γ. This finding agrees qualitatively to the 2D PIC simulation results,[14] which has showed that the enhancement of the 2D LB law for convergent flow is larger than divergent flow. In the range of $\Gamma=3-10$ and $0.2<W/r_2<5$, their PIC simulation results for both divergent and convergent flows were numerically fitted with an empirical formula of $1+0.1536/(W/r_2)+0.0183/(W/r_2)^2$ to within 2.5% for all simulation data. Even though the empirical fitting is reasonably good for both convergent and divergent flows, the enhancement is found to be always larger for the convergent flow at a fixed value Γ

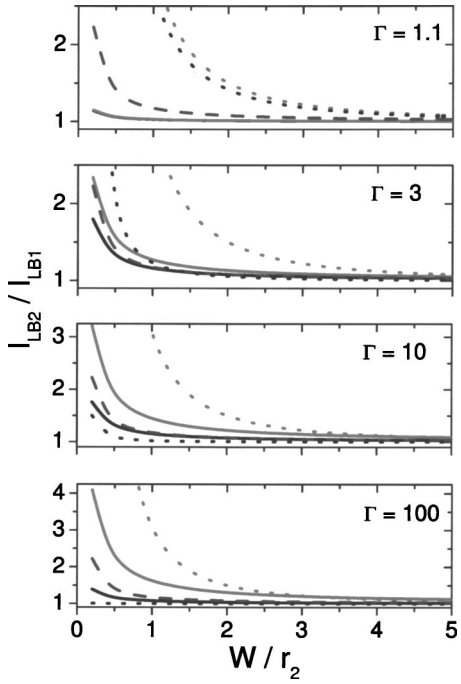

FIG. 4. (Color online). The enhancement of 2D Langmuir–Blodgett (LB) law (in terms of 1D LB law) as a function of W/r_2 for convergent flow (top) and divergent flow (bottom) at various $\Gamma=1.1$, 3, 10, and 100. The dash lines are from the numerical fitting from 2D PIC simulation (Ref. 14): $1+0.1536/(W/r_2)+0.0183/(W/r_2)^2$. The dotted lines are from the analytical formulas (Ref. 15): $1+2/(W/r_2)^2$ for convergent flow (top) and $1+2/(W/r_2)^2/\Gamma^2$ for divergent flow (bottom).

and W/r_2, as shown in their PIC simulation results (see Fig. 3 in Ref. 14), and the difference can be significant at small $W/r_2(<1)$ and at large $\Gamma(=10)$.

To compare with the empirical formula, Eq. (15) is rewritten as

$$\frac{I_{\mathrm{LB}}(2\mathrm{D})}{I_{\mathrm{LB}}(1\mathrm{D})}=1+\frac{4/\pi}{W/r_2}\frac{\Gamma-1}{\Gamma}F(\Gamma,\epsilon). \tag{16}$$

Figure 4 shows the enhancement of 2D LB law $I_{\mathrm{LB}}(2\mathrm{D})/I_{\mathrm{LB}}(1\mathrm{D})$ as a function of $0.2<W/r_2<5$ for various $\Gamma=1.1$, 3, 10, and 100 (top to bottom). The solid lines are the calculated results at $\epsilon=0$ for the convergent flow (top) and the divergent flow (bottom). The dash lines are the numerical fitting of 2D PIC simulation,[14] which is $1+0.1536/(W/r_2)+0.0183/(W/r_2)^2$. It is obvious that the numerical fitted 2D LB law (dashed line) is no longer accurate at small $\Gamma\approx 1$, which should recovers to 2D CL law (for a planar case). For example, both convergent and divergent flows are nearly identical at $\Gamma=1.1$ as shown in the figure. For comparison, recent analytical scalings[15] of $1+2/(W/r_2)^2$ (for convergent flow) and $1+2/(W/r_2)^2/\Gamma^2$ (for divergent flow) are also plotted (dotted lines). Their scalings show poor agreements with the PIC simulation data (dashed lines) (Ref. 14) and our results (solid lines).

It is important to note that our results are only valid for large $W/r_2>1$. Using overinjection method at uniform emission condition, we compare our PIC simulation data with numerical results at $W/r_2=3$ for $\Gamma=1.1-10$, which are plotted in Fig. 5. From the figure, we see that the 2D LB law of

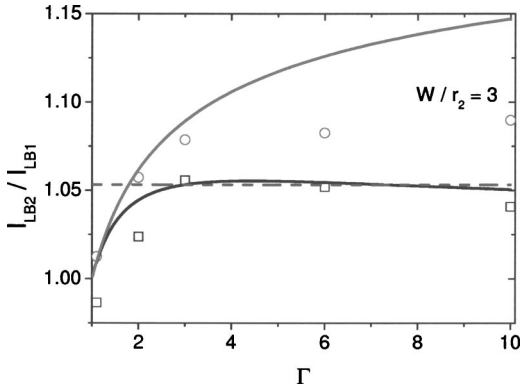

FIG. 5. (Color online). The enhancement of 2D LB law (in terms of 1D LB law) as a function of Γ (=1.1 to 10) for convergent flow (top) and divergent flow (bottom) at various $W/r_2=3$. The dash lines are from the numerical fitting from 2D PIC simulation (Ref. 14): $1+0.1536/(W/r_2)+0.0183/(W/r_2)^2$. The symbols are PIC simulation: convergent flow (○) and divergent flow (□).

the convergent flow is always larger than the divergent law. The agreement of our results is good to within 5% for all simulation data at $W/r_2=3$, but the difference can be as large as 10% at $W/r_2=1$ and $\Gamma=10$ (not shown).

III. REMARKS

The studies of CL law in quantum regime is relatively new, and only the quantum mechanical effects in longitudinal directions are considered in the 1D quantum CL law.[5–7] From the 1D quantum model,[6] it is found that the width of the potential barrier (for electron tunneling in the gap) is smaller than the gap spacing D at space charge limited condition. Thus, the quantum effects in the transverse direction may be ignored when the size of emitting strips (on the cathode) L is large, i.e., $L>D$, as studied in this paper. However, an exact 2D or 3D formulation of quantum CL law is required to fully account for the quantum effects at $L\leqslant D$.

For the relativistic regime, the model is expected only to be valid for weakly relativistic regime at sufficiently small value of U, when the effects of self-magnetic field can be ignored. Including self-magnetic field is extremely difficult analytically, especially when the electron beam is *not* fully insulated in the pinched regime,[17,18] or at cross-field geometry when the self-magnetic field can become important even at significantly low voltage such as 300 kV. The simple 3D relativistic CL law presented in this paper is to serve as an extension of the well-known 1D relativistic CL Law[3] to account for the effects of finite emission area, but ignoring the self-magnetic field. It is important to note that a fully analytical relativistic CL law remained unsolved.

The scalings presented in this paper are valid only for large emission area where the characteristic lengths of the emitting patches are comparable or larger than the gap spacing. Under this assumption, the enhancement of 1D CL law can be split into two separate terms (F and G) as shown in Eq. (2), which account for the physics of electron flow and geometrical properties of the emitting patch on the cathode, respectively. At small emission area, the CL law of a very narrow beam has been recently calculated in the classical

regime for cold electron emission from an infinitely long emitting patch.[19] It will be interesting to see if the results of this paper can be extended to small emission area (for a single sharp emitter), which will be important to study the transition of Fowler–Nordheim law to space-charge limited flow. In studying the transition, the quantum effects of the electron flows near to the tip of the emitter is critical, which will require 2D or 3D quantum mechanical calculations that is beyond the scope of this paper.

IV. SUMMARY

In summary, we have presented a 3D Child–Langmuir (CL) law in the classical, weakly relativistic and quantum regime for uniform hot electron emission in planar and cylindrical configurations. The enhancement of the 3D CL law (in terms of 1D CL law) in all three regimes is formulated in a general form of $1+F\times G$, where G depends on the geometrical properties of the emitting patches on the cathode, and F depends on the 1D electron flow in the gap. The dependence of F is calculated numerically as a function of gap spacing, gap voltage, finite emission energy, and curvatures of the electrodes. The analytical expressions of G are given for various emitting patches, such as rectangle, ellipse, square, circle, and polygons, which are confirmed with 3D PIC simulation. For a cylindrical gap of finite length, it is found that the space charge limiting current for the convergent flow (cathode outside) is larger as compared to the divergent flow (cathode inside). Finally, the 3D CL law model is independent of the cathode materials as in the 1D CL law.

ACKNOWLEDGMENTS

This work was partly supported by the Agency for Science, Technology and Research of Singapore (Grant No. 042 101 0080). One of the authors (L.K.A.) would like to acknowledge the support of Los Alamos National Laboratory operated by the University of California for U.S. Department of Energy when he was a visiting scientist during the course of this work.

[1] C. D. Child, Phys. Rev. **32**, 492 (1911); I. Langmuir, *ibid.* **2**, 450 (1913).
[2] G. Jaffe, Phys. Rev. **44**, 91 (1944).
[3] H. R. Jory and A. W. Travelpiece, J. Appl. Phys. **40**, 3924 (1969).
[4] I. Langmuir and K. Blodgett, Phys. Rev. **22**, 347 (1923).
[5] L. K. Ang, T. J. T. Kwan, and Y. Y. Lau, Phys. Rev. Lett. **91**, 208303 (2003); Phys. Rev. E **64**, 017501 (2001).
[6] L. K. Ang, Y. Y. Lau, and T. J. T. Kwan, IEEE Trans. Plasma Sci. **32**, 410 (2004).
[7] Y. Y. Lau, D. Chernin, D. G. Colombant, and P.-T. Ho, Phys. Rev. Lett. **66**, 1446 (1991).
[8] Y. Y. Lau, Phys. Rev. Lett. **87**, 278301 (2001).
[9] J. W. Luginsland, Y. Y. Lau, and R. M. Gilgenbach, Phys. Rev. Lett. **77**, 4668 (1996).
[10] J. W. Luginsland, Y. Y. Lau, R. J. Umstattd, and J. J. Watrous, Phys. Plasmas **9**, 2371 (2002).
[11] A. Rokhlenko and J. L. Lebowitz, Phys. Rev. Lett. **91**, 085002 (2003).
[12] R. J. Umstattd and J. W. Luginsland, Phys. Rev. Lett. **87**, 145002 (2001).
[13] J. J. Watrous, J. W. Luginsland, and M. H. Frese, Phys. Plasmas **8**, 4202 (2001).
[14] K. G. Kostov and J. J. Barroso, Phys. Plasmas **9**, 1039 (2002).
[15] X. Chen, J. Dickens, L. L. Hatfield, E.-H. Choi, and M. Kristiansen, Phys. Plasmas **11**, 3178 (2004).
[16] B. Goplen, L. Ludeking, D. Smithe, and G. Warren, Comput. Phys. Commun. **87**, 54 (1995).
[17] M. Lopez, Y. Y. Lau, J. W. Luginsland, D. W. Jordan, and R. M. Gilgenbach, Phys. Plasmas **10**, 4489 (2003).
[18] S. B. Swanekamp, R. J. Commisso, G. Cooperstein, P. F. Ottinger, and J. W. Schumer, Phys. Plasmas **7**, 5214 (2000).
[19] A. Rokhlenko and J. L. Lebowitz, Phys. Plasmas **11**, 4559 (2004).